Mohammad-Reza Alam
Madjid Fathi *Editors*

Integrated Systems: Data Driven Engineering

Integrated Systems: Data Driven Engineering

Mohammad-Reza Alam · Madjid Fathi
Editors

Integrated Systems: Data Driven Engineering

Editors
Mohammad-Reza Alam
Department of Mechanical Engineering
University of California
Berkeley, CA, USA

Madjid Fathi
Institute for Knowledge Based Systems
and Knowledge Management
Research Center for Knowledge
Management and Intelligent Systems
University of Siegen
Siegen, Germany

ISBN 978-3-031-53651-9 ISBN 978-3-031-53652-6 (eBook)
https://doi.org/10.1007/978-3-031-53652-6

© The Editor(s) (if applicable) and The Author(s), under exclusive license to Springer Nature Switzerland AG 2024

This work is subject to copyright. All rights are solely and exclusively licensed by the Publisher, whether the whole or part of the material is concerned, specifically the rights of translation, reprinting, reuse of illustrations, recitation, broadcasting, reproduction on microfilms or in any other physical way, and transmission or information storage and retrieval, electronic adaptation, computer software, or by similar or dissimilar methodology now known or hereafter developed.
The use of general descriptive names, registered names, trademarks, service marks, etc. in this publication does not imply, even in the absence of a specific statement, that such names are exempt from the relevant protective laws and regulations and therefore free for general use.
The publisher, the authors and the editors are safe to assume that the advice and information in this book are believed to be true and accurate at the date of publication. Neither the publisher nor the authors or the editors give a warranty, expressed or implied, with respect to the material contained herein or for any errors or omissions that may have been made. The publisher remains neutral with regard to jurisdictional claims in published maps and institutional affiliations.

This Springer imprint is published by the registered company Springer Nature Switzerland AG
The registered company address is: Gewerbestrasse 11, 6330 Cham, Switzerland

If disposing of this product, please recycle the paper.

Preface

The term "integrated system" refers to a seamless collaborative operation of a large number of (potentially unrelated) subsystems to achieve a specific goal. It involves combining multiple subsystems or components, such as hardware, software, networks, and workflows, into one larger system that works as a whole. Integrated systems, widely employed across various scientific and technological domains today, aim to enhance coherence, efficiency, and the overall quality of the system functionality.

A familiar example of an integrated system is a smartphone, which, to deliver the expected smooth functionality, must have a consistent and flawless integration of various subsystems such as electronics, wireless technology, camera, software, user interface, energy management, heat control, smart materials and composite design, ergonomics, and more. Back in the old days, creation of most goods relied mainly on the skills of a single, or small group of artisans, with one (usually specific) expertise. A carpenter, for example, could craft most of the household items. In today's world, however, a lot more is expected from a product than a mere functionality. Take a simple chair, for example. Modern chairs are expected to be ergonomic, necessitating extensive research into people's habits and the health implications of factors like shape, height, and back angle adjustments. Furthermore, factors such as stability, quality, reliability, safety, production methodology, economic considerations, market competition, environmental impacts, and more must also be taken into account for a successful venture.

The concept of "integrated systems" extends beyond consumer products and applies to most modern challenges in science, technology, and society. Astrophysics, for instance, relies on precise measurements primarily accomplished through highly accurate space telescopes fabricated using advanced manufacturing methods. Once constructed the entire telescope must be transported into orbit using efficient and powerful rockets. In the realm of medicine, surgical procedures increasingly depend on a variety of precision machines, ultrasonic devices, X-rays, MRIs, and modern nuclear technologies, bringing together various fields of science and engineering.

As evident from the examples above, the swift pace of technological advancement has heightened the demand for multidisciplinary approaches to tackle intricate

and complex challenges of the modern world. In response, a successful strategy is the integration of systems and technologies that involves combining elements like human resources, technology, and environmental factors to attain a shared objective. Integrated systems and technologies yield numerous advantages, including increased efficiency, enhanced accuracy, higher flexibility, learning capability, adaptability of digital system, superior decision making, and cost savings. Through process streamlining, waste reduction, and overall efficiency improvement, integrated systems and technologies offer a more comprehensive and effective approach to problem-solving.

Despite these advantages, there are still challenges and gaps in our understanding of how to effectively integrate various systems. These challenges include complexity, compatibility, security, cost, resistance to change, customized maintenance, and the need for regular updates while ensuring continued consistency. Addressing these challenges requires a collaborative approach that brings together experts from different fields to develop effective solutions. Enterprises and industrial parties must also stay vigilant and informed about key technologies in their respective fields and beyond to identify opportunities for integrating different technologies and systems.

The Integrated Systems Design and Technology (ISDT) conference aims to facilitate collaboration among diverse disciplines in various sectors. The event features renowned scientists from around the globe who specialize in a wide range of fields, with the goal of fostering a deeper understanding of other disciplines and the approaches required for multidomain research and projects. The theme of 2023 conference revolved around the pivotal role of data in engineering and knowledge technology. As technology continues to advance, data driven approaches have become increasingly critical in shaping the future of engineering design and production. This year's conference aimed to delve into the various ways in which data and knowledge can be utilized to enhance and optimize engineering processes, improve precision, and facilitate innovation.

The ISDT community is committed to establishing a network of professionals worldwide to foster international collaboration. This network will facilitate the exchange and sharing of ideas, best practices, and innovations among experts from different disciplines, resulting in the development of effective solutions for complex challenges, including those encountered in Industry 4.0 and Society 5.0. By bringing together scientists from different fields, ISDT aims to promote interdisciplinary collaboration and innovation, ultimately yielding improved outcomes and more efficient problem-solving.

Berkeley, CA, USA Mohammad-Reza Alam
Siegen, Germany Madjid Fathi

Contents

Knowledge-Based Learning

Automated Photonic Waveguide Loss Measurement Using Out-scattering Light Method 3
Xiangjian Zeng, Jay W. Reddy, and Maysamreza Chamanzar

Interpretable Prototype Discovery in Deep Learning-Based Time Series Classification 25
Gaurav R. Ghosal and Reza Abbasi-Asl

One-Shot Defect Fingerprint Comparability Using Siamese Networks for Wafer Map Similarity in Semiconductor Manufacturing 35
Christian Weber, Sathvik Dembale Krishnappagowda, Ralf Montino, Peter Czerner, and Madjid Fathi

Opportunities of Data Driven Medicine: Collection, Transfer, and Processing of Vital Data in Outpatient Care 63
Alexander Keil, Rainer Brück, Kai Hahn, and Olaf Gaus

Performance and Optimisation of Microfluidic Channels with Acute Angles and Serpentine Curvatures 83
Mozafar Saadat, Arran Hughes, Alexander Jungclaussen, Amir Hajiyavand, Gowsihan Poologasundarampillai, Amirpasha Moetazedian, and Majid Malboubi

Swimming Robots for Targeted Chaotic Mixing in Viscous Environments 101
Mehdi Mirzakhanloo, Mohsen Saadat, Mir Abbas Jalali, and Mohammad-Reza Alam

Intelligent Robotics and Embedded Controls

Adaptive Hierarchical Meta-Scheduling for Distributed Time-Triggered Systems with Diverse Internal and System Architectures 117
Pascal Muoka, Tom Kiesow, Daniel Onwuchekwa, and Roman Obermaisser

Cognitive Controllable Local System Improving Blackstart Resilience in Smart Distribution Grids 135
Kai Daniel, Daniel Henn, and Daniel Kurzer

Real-Time Anomaly Detection in Connected Autonomous Vehicles: A Data-Driven Approach 147
Mahsa Jalali, Milad Moradi, and Mehdrad Saif

MASTER-XR: Mixed Reality Ecosystem for Teaching Robotics in Manufacturing 167
Michael Barz, Panagiotis Karagiannis, Johan Kildal, Andoni Rivera Pinto, Judit Ruiz de Munain, Jesús Rosel, Maria Madarieta, Konstantina Salagianni, Panagiotis Aivaliotis, Sotiris Makris, and Daniel Sonntag

Semantically Enriched Interfaces for Product Configuration 183
Stefan Berlik, Philipp Hartmann, and Jannick Stranghöner

Knowledge Technology in Material Engineering

Recent Progress on Effect of Different Parameters on Thin Films for Enhanced Superconducting Properties 197
Navid Nasajpour-Esfahani, Hamid Garmestani, Ngoc L. Tran, Yuzhou Chen, Elnaz Jamshidi, As'ad Alizadeh, and Reza Nabiun

Intelligent Lumber Production (Sawmill 4.0): Opportunities, Challenges, and Pathways to Adoption 213
Vahid Nasir, Sohrab Rahimi, Ahmad Mohammadpanah, Eric Hansen, and Farrokh Sassani

Polymer-Based Nanocomposites for Tissue Engineering: Surface to Bulk Structural Design 233
E. Tamjid

Knowledge-Based Design and Fabrication of Advanced Composites and Hybrid Materials for Nanomedicine 249
A. Simchi and P. Kianfar

TExKG in Health Domain: The Application of Knowledge Graph Based Framework for Explainable Recommendations in the Contexts of Elderly Care, Mental Health, and Emergency Responses 265
Hasan Abu-Rasheed, Mubaris Nadeem, Mareike Dornhöfer, Johannes Zenkert, Christian Weber, and Madjid Fathi

Intelligent Sustainability

Data-Driven Identification and Control of Positive Systems 289
Yueyang Wang and Bahram Shafai

Real-Time Ocean Prediction via a Grid of Autonomous Self-powered Swarm of Ocean Sensors 309
Prashant Chandra Pujari, Aneesh Jois, Jacob Lim, Stephanie Popielarz, Jianxi Wang, and Mohammad-Reza Alam

Integrated System Approach for Peer-Peer Energy Trading 327
Hector K. Lopez and Ali Zilouchian

Innovation and Design Model in Marine Decarbonization Activities 343
Zuhal ER

Knowledge-Based Learning

Automated Photonic Waveguide Loss Measurement Using Out-scattering Light Method

Xiangjian Zeng, Jay W. Reddy, and Maysamreza Chamanzar

Abstract Characterization of optical waveguide propagation loss is fundamental to the practical realization of integrated photonics. Evaluating waveguide performance throughout the fabrication process enables rigorous quality control and rapid fabrication process development and optimization. Conventional measurement techniques such as the cutback and modified cutback methods directly measure the out-coupling light intensity from optical fibers and photonic waveguides of different lengths, and subsequently estimate the waveguide propagation loss. These methods are generally laborious, requiring many measurements for each device. Additionally, they are destructive to the device under test, as in the case of the cutback method, or require specially-designed arrays of various lengths, as in the case of the modified cutback method. In this work, we describe a method utilizing the out-scattering light intensity profile to efficiently assess multiple waveguides non-destructively and in a fully-automated manner to determine the individual waveguide propagation loss and identify faulty waveguide regions. The accuracy of the out-scattering method is validated using traditional modified cutback methods. Moreover, a comparative analysis of the two methods is presented, along with strategies to optimize their performance. This study is performed using Parylene photonic waveguides, which we have recently demonstrated for light delivery into the brain for neural stimulation.

X. Zeng · J. W. Reddy · M. Chamanzar (✉)
Department of Electrical and Computer Engineering, Carnegie Mellon University, 5000 Forbes Ave, Pittsburgh, PA 15213, USA
e-mail: mchamanz@andrew.cmu.edu

X. Zeng
e-mail: xiangjiz@andrew.cmu.edu

J. W. Reddy
e-mail: jreddy1@andrew.cmu.edu

© The Author(s), under exclusive license to Springer Nature Switzerland AG 2024
M.-R. Alam and M. Fathi (eds.), *Integrated Systems: Data Driven Engineering*,
https://doi.org/10.1007/978-3-031-53652-6_1

1 Introduction

Optical waveguides are widely utilized in domains such as optical communications, integrated photonics, and biophotonics [1, 2]. A fundamental property of an optical waveguide is how quickly the optical power decays as light propagates through the waveguide (i.e., the propagation loss). The propagation loss ultimately determines the suitability of a given waveguide architecture for its intended application, depending on the requirements for the input/output power and the length of the waveguide. Therefore, characterizing the waveguide propagation losses is an essential part of quality control and performance optimization.

Numerous waveguide propagation loss characterization methods have been demonstrated in the past. The direct cut-back method, in which a manufactured waveguide is cut shorter sequentially for each output power measurement, provides a straightforward probe into propagation loss by measuring the optical power attenuation between each measurement [3]. However, such an approach is destructive to the waveguide sample and hence undesirable under many circumstances. For instance, in a research setting, fabricating many samples for repeated measurements can be inefficient. In addition, in a production line, destructive testing can only be used for spot-checking quality control, but can’t be used to validate the performance of every single device before use. The latter is especially problematic for critical systems, i.e., in biophotonics, where a defective device can put an implanted animal model or human being at risk.

To preserve the samples under test, the modified cut-back method compares the output light intensity of multiple waveguides with different lengths [4]. However, these measurements require repeated alignment to many waveguides, which can introduce experimental error from trial-to-trial variance. Additionally, it requires specially-designed cutback structures of various lengths to be fabricated. Furthermore, it only measures the average propagation loss across a group of waveguides, meaning that the measurement accuracy will suffer from device-to-device variations, as well as variations in the coupling efficiency. Although cutback methods are the most prevalent, various other measurement techniques have been introduced in recent years to address their limitations, including using ring resonators [5], Fabry-Pérot resonators [6–8], and electro-optic Mach-Zehnder interferometers [9] to estimate the propagation loss. Although these techniques are nondestructive and accurate, they nonetheless require the construction of a specialized structure in order to measure the propagation loss in an equivalent waveguide. Consequently, they cannot assess the in-situ performance of a functional device. More importantly, the performance characteristics of functional devices must be inferred from the specialized device under test, so these methods are poorly suited for characterizing the intra-batch variance during the fabrication, or for isolating localized defects within a single sample waveguide. To fill the gap of these existing methods, there is an outstanding need for a method to allow the accurate, high-throughput, in-situ characterization of the waveguide propagation losses.

Due to the above constraints, the out-scattering method has been explored as a way to improve waveguide propagation loss characterization capabilities [10]. By observing the intensity profile of out-scattering light, this method estimates the optical power decay within the waveguide with high spatial resolution while being nondestructive. The propagation loss of individual regions within the waveguide can be obtained by a localized measurements of out-scattering light. Additionally, this method directly observes the waveguide itself, without the need for specialized structures. Because of these benefits, the out-scattering method has seen increasing used in recent years [11–14].

However, key limitations to the out-scattering method have prevented its widespread adoption. The reliability of the out-scattering method hasn't been validated using a rigorous comparison to the gold-standard techniques such as the cutback method. Prior published work has shown that the out-scattering light method and modified cutback method have good agreements for some cases [15]. However, to the best of the authors' knowledge, there has not been extensive characterization of the regime under which out-scattering light methods can be considered reliable. In addition, the out-scattering light technique doesn't inherently eliminate problems of repetitive re-coupling for each waveguide. These two issues need to be addressed to render the out-scattering method suitable for wider adoption.

Here, we demonstrate the out-scattering method to characterize Parylene photonic waveguides. Parylene photonics is a flexible biocompatible material platform for biophotonic devices such as implantable optical brain-computer interfaces. Previous work has shown that the fabrication of low-loss (i.e., < 5 dB/cm) Parylene photonic waveguides requires optimized etching conditions and an additional smoothing step to reduce scattering losses [13]. Since the out-scattering method is non-destructive, it may be used for intermediate process characterization between individual fabrication process steps, i.e., before the smoothing step to characterize the waveguide performance in the middle of the fabrication process. This technique was previously used to characterize Parylene photonic waveguide performance [14] demonstrating losses of (3.2 dB/cm at $\lambda = 680$ nm, 4.1 dB/cm at $\lambda = 633$ nm, 4.9 dB/cm at $\lambda = 532$ nm, 6.1 dB/cm at $\lambda = 450$ nm) after smoothing. Here, we provide a detailed description of the out-scattering method and demonstrate its utility for wafer-scale characterization during intermediate steps of the fabrication process.

In this work, we validate the out-scattering light method by performing a rigorous characterization of integrated photonic waveguides using both the out-scattering light and modified cutback methods. Furthermore, we provide guidelines and constraints on when to utilize the out-scattering light method in order to obtain accurate results. This out-scattering characterization method, combined with a custom-designed hardware and software system enables high-throughput and fully-automated measurement of photonic waveguides on the wafer scale.

2 Method

To perform a rigorous comparison of the out-scattering method and the modified cutback method for assessing propagation loss, we constructed a custom-built robotic characterization system to perform high-throughput and low-variance measurements of micro-fabricated integrated photonic waveguides on the wafer scale (Fig. 1). A custom software pipeline was built to perform the automated measurements as well as the analysis. In this section, both the waveguide wafer design and acquisition setup are explained in detail. Subsequently, we discuss the software system and techniques for automated fiber alignment and imaging to obtain waveguide path images for propagation loss fitting. Finally, the experimental procedures for two propagation loss measurement methods—the modified cutback method and the out-scattering method—are presented.

2.1 Waveguide Fabrication

In this work, we utilized the micro-fabricated Parylene photonic waveguides as testing samples to validate the performance of the proposed method. Here, a specific wafer layout is designed to facilitate the measurement process.

Parylene photonic waveguides were fabricated using the microfabrication process described in [14]. Briefly, 45-degree micromirror molds are etched in a silicon wafer at the input and output ports of the waveguides via anisotropic KOH etching to enable out-of-plane input and output coupling. Low refractive index polydimethylsiloxane (PDMS) is spin-coated as a lower cladding of the waveguides to a thickness of 1 μm, and high-index Parylene C is deposited via chemical vapor deposition to a thickness of 3.5 μm across the wafer surface, then etched in oxygen plasma to form the waveguide core using a lithographically-defined Chromium hard mask. Notably, to demonstrate the feasibility of nondestructive wafer-scale characterization of the waveguides during an intermediate process step, measurements are performed midway through the process–before depositing the subsequent loss-reducing Parylene C smoothing layer described in previous work [13, 14] is applied.

For the purposes of the analyses performed in this paper, we utilize a wafer layout that can be measured via either the modified cutback method or the out-scattering method. This design allows results for both methods to be collected from the same samples to verify the accuracy of the out-scattering method. The wafer layout contains 200 waveguides in total. The waveguides are organized in groups of 20 waveguides of the same length. Each group contains 4 sets of 5 waveguides with widths of 5 μm, 10 μm, 15 μm and 30 μm each. Each group of 20 waveguides are referred to as a waveguide batch and are linearly arranged on the wafer so that all of the input and output ports are aligned. Each subsequent batch of waveguides (5 mm longer) is placed adjacent to the previous batch, protruding 2.5 mm longer in both directions. This pattern is iterated until the 10th batch of waveguides reaches 50 mm

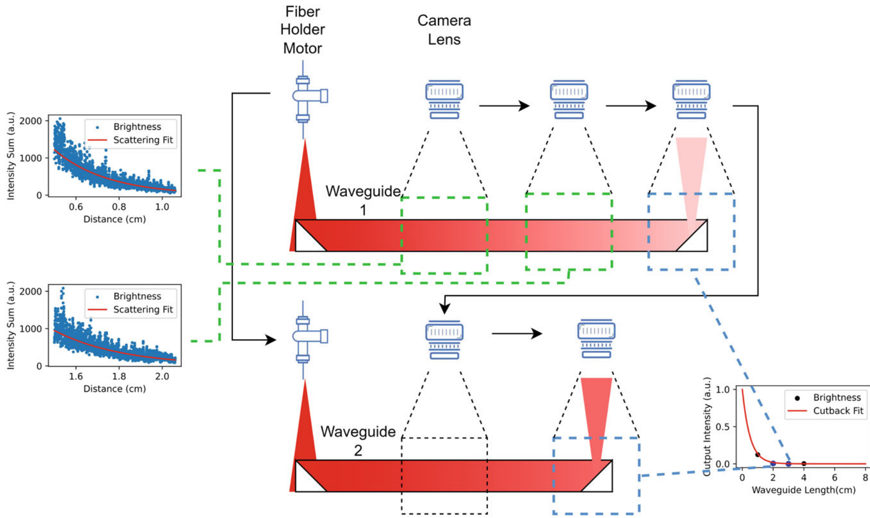

Fig. 1 Diagram showing the full waveguide characterization pipeline. Initially, the input optical fiber is aligned to a single waveguide input, and the camera traverses the entire length of the waveguide to capture multiple images for out-scattering light loss measurements, which are shown in inset plots to the left. Once the out-scattered light of the entire waveguide has been measured, the output intensity is captured. The fiber is then moved to align to the next waveguide. The process is repeated until all waveguides are imaged. Multiple output measurements from waveguides of different lengths can be used to calculate the loss via the modified cutback method, which is shown in the inset figure on the right

in length, providing a range of waveguide lengths to measure. Each waveguide on the wafer features monolithically-integrated micromirrors at the waveguide input and output ports to enable out-of-plane input and output coupling. Out-of-plane output coupling permits both the output port and out-scattering light path to be observed by a vertically-oriented camera, whereas out-of-plane input coupling allows coupling to a vertically-oriented input optical fiber. As will be discussed in later sections, a sufficiently long waveguide is essential for obtaining accurate results with the out-scattering method. In this work, we have tailored our experimental protocol to our particular wafer layout design. However, in principle, this method is generalizable to any wafer that features out-of-plane coupling and waveguides of various lengths.

2.2 Acquisition Setup

To achieve robust, high throughput measurements, the waveguide characterization system is capable of automatically observing and adjusting the alignment of this input optical fiber onto the wafer via the integrated camera and motorized stages.

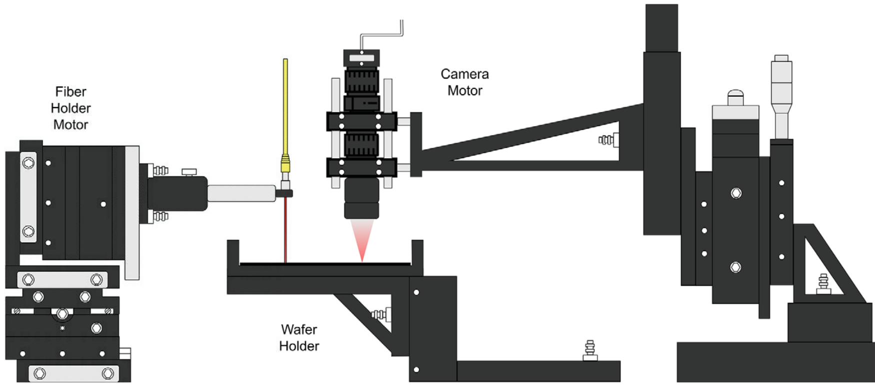

Fig. 2 Diagram of the automatic characterization system, including the wafer holder, fiber holder motor system, and camera motor system. The wafer containing waveguides being characterized is secured using a 3D printed wafer holder. The fiber holder motor positions the fiber to couple light into the waveguide. The camera captures images for both automated alignment and automated imaging steps in the acquisition pipeline

The waveguide characterization system consists of three modules: (1) wafer holder, (2) fiber holder stage and motor system, and (3) camera stage and motor system (Fig. 2). The fiber holder motor and camera holder motor each can move in the XYZ directions, and the camera holder can additionally rotate along the center axis. The input optical fiber is fixed in a vertical orientation above the wafer surface by the fiber holder. The fiber motor allows the fiber to not only travel in X and Y direction to align with individual waveguides, but also to adjust the distance to the wafer surface to efficiently couple to the waveguide input port. Light is coupled into the waveguides from a 633 nm 50 mW pigtailed laser diode (LP633-SF50, ThorLabs). Likewise, the camera holder moves the camera to locate and capture the output ports of the waveguides, while the rotation allows the camera to pivot to prevent collision with the input optical fiber while imaging near the input port. The camera system used for imaging consists of a CCD Camera (EO-5012M, Edmund Optics) and VZM^{TM} 600i Zoom Imaging Lens with a 60 mm working distance. This CCD camera was chosen since it provides low noise imaging in low-light conditions. The chosen lens provides an adjustable field of view (1.0–6.4 mm), suitable to image small segments of the waveguides (5–50 mm long).

For each round of measurements, the waveguide wafer under test is secured using a 3D printed wafer holder. The initial position of the fiber holder is manually set to ensure all waveguides fall within the motor travel range.

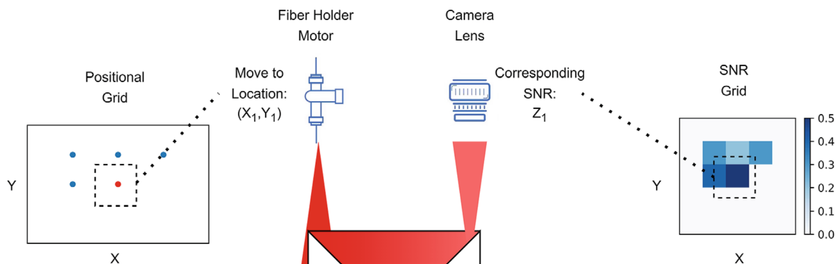

Fig. 3 Diagram of the automated alignment step. The fiber holder scans through a grid to find the optimum coupling position. For each position, an image containing waveguide path is taken by the camera to evaluate the signal-to-noise ratio (SNR). The system chooses the position corresponding to the highest SNR value for subsequent automated imaging

2.3 Acquisition Pipeline

After securing the waveguide wafer and setting the initial fiber location, the software system begins the image acquisition pipeline for each waveguide, which consists of two phases: automated alignment and automated imaging.

During automated alignment, the system couples the fiber to the micro-mirror input port of the waveguide to maximize output intensity (Fig. 3). The fiber holder scans a positional grid around the starting location while monitoring the waveguide out-scattering brightness to discover the optimal waveguide coupling position, as described in our previous publication [16]. The system performs three rounds of grid search around the optimal coupling position with decreasing grid spacing each time to gradually approach the optimum coupling position. For our waveguide with a width of up to 30 μm, we chose 6 μm, 1 μm, and 0.2 μm grid spacing for each iteration and 6 by 4 grid positions in X and Y directions. For each position the holder moves to, the camera captures one image containing out-scattering light 5 mm from the input port.

In our previous work [16], we used the intensity sum along the waveguide path as a measure of the coupling quality. Further investigation showed that the previous strategy would favor images with strong stray light reflections from the input port (Fig. 4 right) over high coupling efficiency (Fig. 4 left).

To overcome this limitation, here the quality of the coupling in each image is evaluated via the Signal-to-Noise Ratio (SNR). Here SNR is defined as the average intensity of pixels in the waveguide path region over the average intensity of pixels in the non-path region (defined as more than 35 pixels away from the waveguide center):

$$SNR = \frac{\frac{\sum_{n \subset WG} I_n}{|n \subset WG|}}{\frac{\sum_{n \notin WG} I_n}{|n \notin WG|}} \qquad (1)$$

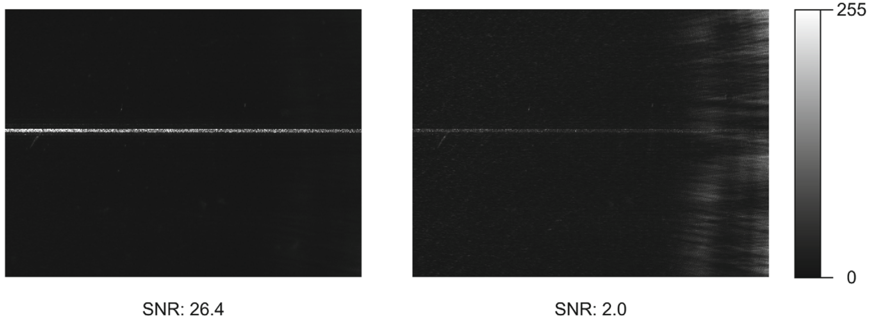

Fig. 4 Comparison between waveguide path image with good coupling (left) and high stray light intensity (right). As shown here, SNR can effectively distinguish the good coupling scenario

The SNR metric helps with the identification of fiber positions with high stray light intensity since the background light intensity is much higher than that of fiber positions with high coupling efficiency. After the positions are ranked, the fiber is moved to the optimal position.

Once the input coupling is optimized, the system proceeds to the automated imaging step. Propagation loss estimation via the out-scattering method requires imaging of regions of interest along the entire waveguide. The system automatically scans through the length of the waveguide, taking piecewise images. Each image covers 5.6 mm of the waveguide length. These piecewise images are offset by increments of 1 mm along the length of the waveguide, yielding a partially overlapping sequence.

Optical power decays exponentially within the waveguide, so the corresponding out-scattering light and intensity at the output port will vary by several orders of magnitude along the length of long waveguides. Thus, it's necessary to automatically adjust the camera exposure time to ensure the image intensity falls within the dynamic range of the camera sensor (0–255 pixel intensity in 8-bit encoding). To perform accurate high dynamic range imaging, we characterized the linearity of the sensor. We projected a 12 μW power laser light directly into the camera lens and varied the exposure time while measuring the peak brightness. As shown in Fig. 5, the peak brightness in the image exhibits nonlinear saturation behavior well before it reaches the peak 255 pixel intensity value. Thus, values in the image close to 255 may underestimate the true brightness level of the waveguide. Intensity ranging between 50 to 200 appears to follow a linear relationship with the exposure. Thus, to ensure linearity across a high dynamic range, the exposure time of the camera is automatically adjusted for each image to maintain a peak pixel intensity between 50–200.

During automated imaging, for each new camera location, a trial image is taken for exposure adjustment. Exposure time is adjusted according to the maximum image intensity via a binary search. If the intensity is greater than 200, then the exposure time is halved; if the intensity is less than 50, the the exposure time is doubled for the next iteration. This process is repeated until an optimum brightness is reached or the

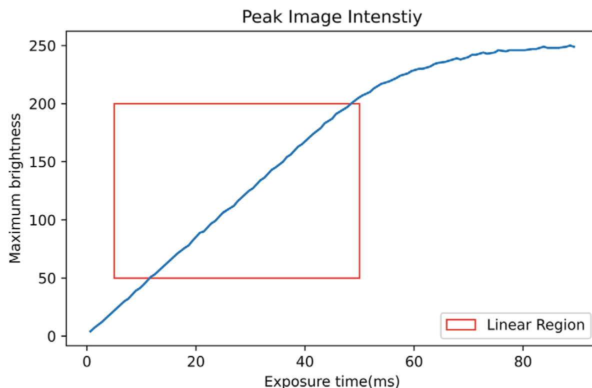

Fig. 5 Pixel intensity does not scale linearly with the exposure time for the CCD camera used in this study. Saturation occurs for intensity values greater than 200, before the dynamic range maximum (255) of the image is reached. The linear region of the sensor is indicated in red

camera exposure time reaches the hardware limit (0.6 µs–2.7 s). The final exposure time is stored alongside each image. In the following analyses, the system utilizes adjusted brightness $I_{adjusted}$ to represent the true brightness of the waveguide, which is a product of the image brightness I_{image} and the camera exposure time $T_{exposure}$:

$$I_{adjusted} = I_{image} \cdot T_{exposure} \tag{2}$$

After the characterization system automatically aligns to and images each waveguide, the fiber and camera motor will move to the position of the next waveguide based on the wafer layout to start another iteration of the acquisition pipeline. Due to the small size of the waveguide port and pitch (less than 40 µm), any in-plane angle mismatch between the fiber motor and wafer axes could significantly impact the movement accuracy and lead to misalignment for the subsequent input ports. Considering uni-directional target movement over distance L, the resultant distance mismatch in two directions given angle mismatch θ should be smaller than half of the maximum search grid range L_G:

$$L \sin\theta < \frac{L_G}{2} \tag{3}$$

$$L(1 - \cos\theta) < \frac{L_G}{2} \tag{4}$$

For our setup with travel distance between waveguide batches of 2.5 mm in X direction, 0.7 mm in Y direction, and a maximum search grid range of 36 µm in X and 24 µm in Y, the tolerance of angle mismatch is 0.27° (Constrained by Y mismatch: $2.5mm \sin\theta < \frac{24\mu m}{2}$), which is infeasible to reliably achieve via manual alignment. Thus, the pipeline employs automatic angle mismatch compensation. As shown in

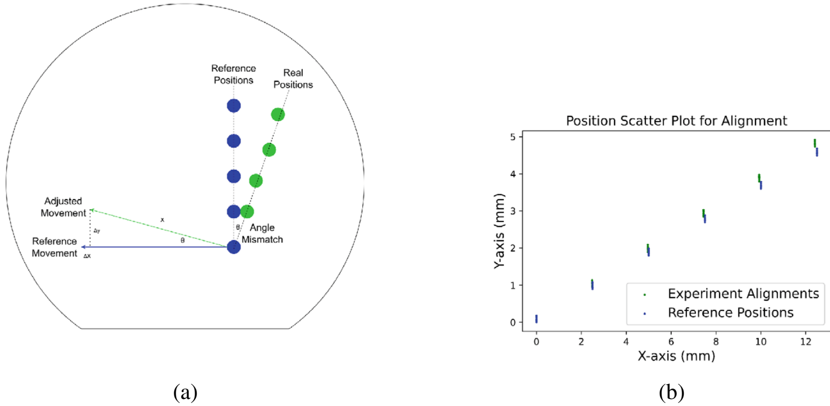

(a) (b)

Fig. 6 **a** After acquisition of waveguides close to the initial fiber position, the actual alignment positions of waveguides on the wafer are captured. These positions are then compared with the reference position from the wafer layout. A mismatch angle θ is computed accordingly, which will be continuously updated for all future motor movements. **b** An example position scatter plot showing the effect of angle adjustment. An alignment trial across 30 waveguides in 6 batches is performed to generate the above plot. The positional difference due to angle mismatch becomes more and more pronounced after each iteration. Thus, angle adjustment is necessary to ensure valid alignment for long-travel-range trials

Fig. 6, after imaging initial sets of adjacent waveguides, the final alignment positions of waveguide input ports are recorded, which are compared to the known wafer layout to calculate the angle mismatch to correct subsequent motor movements. To learn the initial wafer orientation, the design features a batch of waveguides of the same length, which are close together (0 µm, 60 µm pitch for X and Y direction respectively). The fiber motor traverses these 5 initial ports that are 240 µm apart without adjustment for an initial orientation estimation. This relaxes the manual alignment constraint to 4.30° (Constrained by X mismatch: $240\mu m \sin\theta < \frac{36\mu m}{2}$). Following this initial batch, the system continually refines its estimate of the rotation mismatch as it aligns to additional waveguides.

Subsequently, the acquisition procedure is iterated until all waveguides of interest on the wafer have been imaged. As in Fig. 6, with this method, the system is able to account for the angle mismatch to perform reliable alignment to many waveguides with input ports distributed across the wafer surface.

2.4 Analysis Pipeline

In order to validate the reliability of the out-scattering method, we performed measurement of the test sample using both the modified cutback method and the out-scattering method and compared their results. In addition, we investigate the per-

formance of both measurement techniques under various imaging conditions and identify criteria (i.e., SNR and waveguide length) to ensure accurate measurement of the device under test.

2.4.1 Modified Cutback Method Fitting

We used the modified cutback method fitting as a reference method to measure the average waveguide propagation loss. The method measures the output intensity of waveguides of different lengths on the same wafer to estimate the propagation loss. Within the waveguide, the light intensity follows an exponential decay:

$$I = I_0 e^{-\alpha L}, \quad (5)$$

where I and I_0 are output and input intensity, L is the light travel distance, and α is the propagation loss of the waveguide. With a constant input intensity, the output intensity will exponentially decay with waveguide length. Here, the output intensity of the waveguide is measured by imaging the output port and calculating the total intensity sum, subject to the linear camera sensor regime discussed previously.

To obtain the output intensity necessary for calculating the propagation loss, the system first identifies the output port in acquired images containing the end of the waveguide. The system uses a predefined output port template to perform template matching to locate the center of the output port [17].

In an initial calibration step that only needs to be performed once per wafer layout, the input fiber is first manually coupled into one waveguide. An image of the output port with out-coupling light is captured, manually cropped to the region of interest, and defined as an output port template (Fig. 7). The template is cross-correlated with the image to obtain the corresponding correlation value map. The maximum value in that map represents the coordinates where the image region best resembles the template and is deemed the center of the output port. Subsequently, a circular mask of radius 22 pixels (empirically chosen to produce repeatable intensity readings from a single waveguide) is defined around the detected center. The final output intensity value is the sum of all pixel brightness values over the mask. Output intensities from different waveguides (of different lengths) are then fitted to an exponential curve to obtain the average propagation loss value of all waveguide batches on the wafer. In this method, we are assuming that different waveguides with the same widths but different lengths have the same propagation loss, which is a good assumption when the variation between the waveguides due to fabrication imperfections is relatively small.

2.4.2 Out-Scattering Method Fitting

The out-scattering method provides an estimation of the propagation loss from individual waveguide images instead of an aggregate estimate from an entire batch of

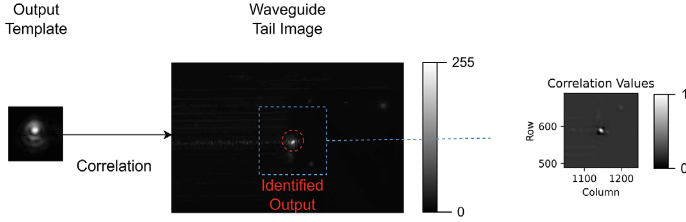

Fig. 7 Template matching to locate the waveguide output in the image. During template matching, predefined output template is cross-correlated pixel-wise with the raw image captured at the end of the waveguide. The maximum correlation value indicates the detected output port coordinates

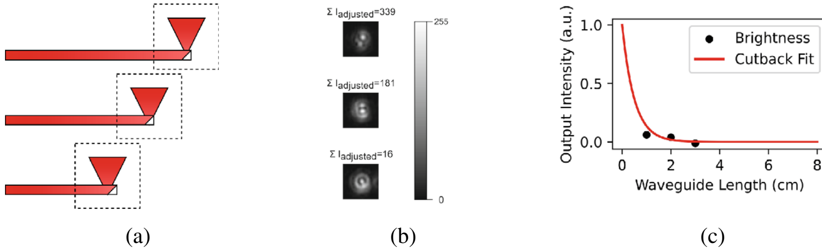

Fig. 8 Pipeline performing the modified cutback method. **a** Example image containing the output region of waveguides under characterization. Output light reflected by the micromirror appears as a bright spot in the recorded image. **b** Output port detection using template matching. Its intensity is summed to measure the optical power. **c** For waveguides with various lengths, their output pixel intensity sums are fitted to an exponential decay to calculate the propagation loss

waveguides (Fig. 8). Here, the out-scattering light from the waveguide is assumed to follow an exponential decay according to the propagation loss. In this analysis, the software utilizes a series of images taken along the waveguide path. For each image, the 1D Hough Transform is applied to identify the waveguide region [18]. In this step (Fig. 9), the image is first thresholded (at 70% of max intensity) to isolate bright pixels of interest. Then, the number of bright pixels is counted row-wise to vote for the waveguide region center row in the image. Its surrounding region containing 70 rows of pixels in total (empirically chosen based on the waveguide width and magnification level) can be identified as the waveguide area in the image. Thus the intensities of the waveguide pixels are summed column-wise to fit an exponential decay curve.

However, captured waveguide images may contain issues that skew the propagation loss measurement. Consequently, more processing is required to obtain an accurate estimate of the propagation loss of waveguides.

First, images captured within 15 mm distance of the input port are observed to have an unusually high propagation loss (Fig. 12). Since such high loss fails to agree with loss measured with the modified cutback method fitting, we hypothesize that it may be related to the out-scattering light associated with the rapid decay of spurious or higher-order modes of the waveguide which possess a higher propagation loss.

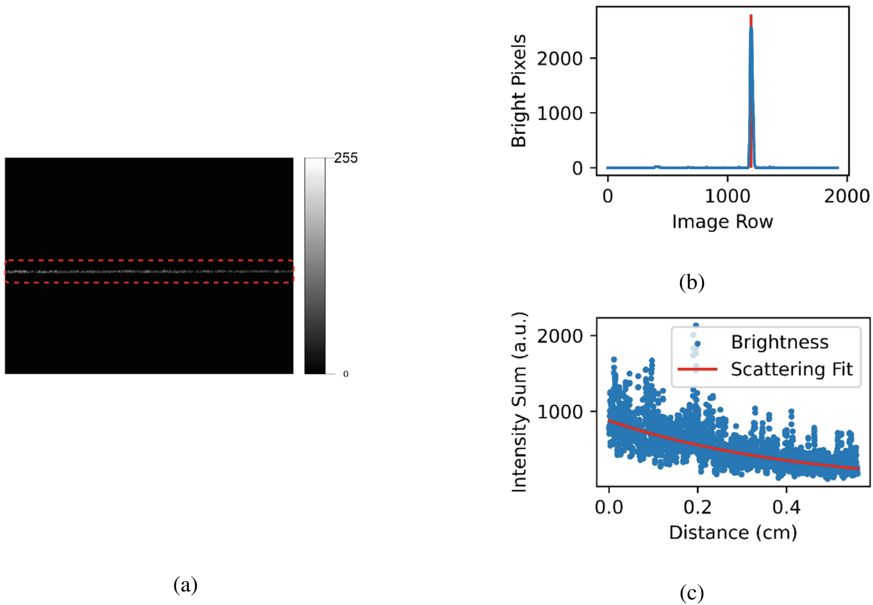

Fig. 9 Out-scattering method fitting on a single waveguide image. **a** Raw image containing the detected waveguide path. **b** 1D Hough transform of the raw image where bright pixels are counted row-wise. The peak row indicates the waveguide center. **c** Out-scattering method fitting result of the shown image. Pixel intensities in the region of interest are summed column-wise and fitted to an exponential decay curve. The fitted out-scattering intensity sum loss corresponds to the overall propagation loss of the waveguide

Some optical power may be coupled into these modes at the input port, but due to their rapid decay, their affect is localized to near the input coupling region. Optical power lost due to coupling into higher-order modes should not be considered when measuring the propagation loss experienced by light that is effectively coupled to efficiently guided lower order modes. Else, the out-scattering fitted propagation loss will be heavily overestimated due to the rapid decay of higher-order mode power in images. Hence, we choose to ignore these near-input images for out-scattering fitting.

Furthermore, we also need to remove artifact-contaminated and faulty waveguide images from fitting since these outliers can skew the overall loss estimates. This step is done by detecting and removing exponential fitting results with R-squared values smaller than 0.4. Lastly, we heuristically remove noisy images with SNR lower than 20 since they tend to underestimate the fitting loss by averaging background noise. A SNR threshold of 20 ensures minimal level of background noise in images, which is shown by numerical simulation to give a high confidence ($p < 0.05$) of accurate estimation within 10% despite noise. Further examples and discussion of these conditions are included in Sect. 3.

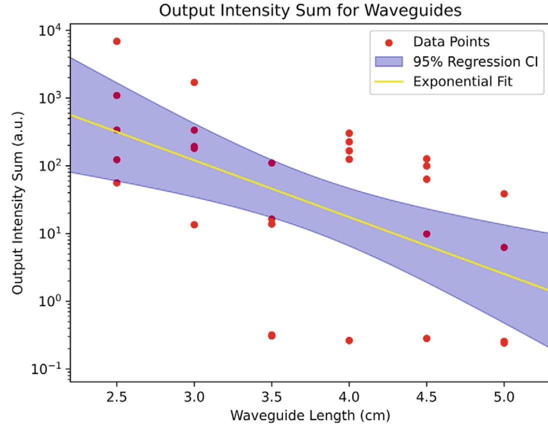

Fig. 10 Modified cutback method fitting result is shown above. 30 total 30 μm wide waveguides were measured (5 each of lengths of 25, 30, 35, 40, 45, and 50 mm). Their output intensity are plotted in red in logarithmic scale. The fitted propagation loss plotted in yellow for the batch was 8.36dB/cm with a 95% confidence interval (CI) of [3.60 dB/cm, 13.19 dB/cm] (CI calculated based on Student's t distribution)

3 Results

To validate the performance of out-scattering method, modified cutback method and out-scattering method were separately used to measure the propagation loss of the same wafer. Individual propagation losses obtained from out-scattering method were in good agreement with that of the modified cutback method. Other factors potentially compounding out-scattering measurement accuracy, such as alignment variance, SNR, and fitting R-squared value, are characterized and addressed in the following section.

3.1 Modified Cutback Method Result

We performed the characterization on the aforementioned wafer containing Parylene photonic waveguides [13]. We imaged thirty 30-μm-wide waveguides ranging from 25 to 50 mm in length. We first obtained results using the modified cutback method. This widely-used method serves as a baseline to evaluate the accuracy of the out-scattering method fitting. The modified cutback method fitting result is shown in Fig. 10. Thirty total waveguides were measured (5 each of lengths 25, 30, 35, 40, 45, and 50 mm). The fitting shows an average loss of 8.36 dB/cm with a 95% confidence interval of [3.60 dB/cm, 13.19 dB/cm] (Fig. 10). Confidence interval is computed as $\overline{x} \pm t \cdot SE \cdot \overline{x}$, where $\overline{x}$, t, SE are mean fitting coefficient, t-score and standard error, respectively.

The wide confidence interval of the modified cutback method fitting is likely due to the large variance in sample measurements. To characterize the automated characterization system measurement accuracy, a repeated alignment trial was performed. The system repeatedly coupled to four waveguides for 20 times each and measured the output port intensity profile. Between each run, a random perturbation up to 2

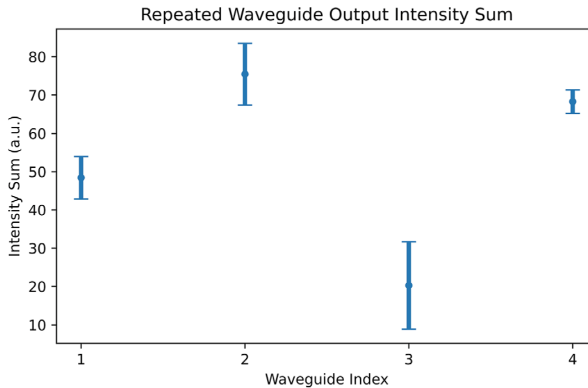

Fig. 11 Repeated alignment over the same waveguides shows the stability of the system. Four waveguides were each aligned to the input port for 20 times each and the corresponding output intensity sum was computed as a measurement of the relative coupling efficiency. Vertical bars indicate the intensity standard deviation for each waveguide. Random perturbation is introduced between each alignment. The average measurement variance of the waveguides is 21%

μm in X and Y direction was imposed on the fiber holder and the input coupling is restored via automated alignment. Figure 11 shows the intensity sum of output profile results. Intensity sum variance was computed for each waveguide based on 20 different measurements. The average variance measured intensity sum for each waveguide is 21%. Thus, there is approximately 1 dB of variance in insertion loss due to automated alignment in the system. Notably, the waveguide-to-waveguide variation is also significant (40%, 2.24 dB), due to device-to-device variation of the fabrication process. Other factors contributing to large variance might also include wafer degradation over time and potential damage to individual waveguides due to particulates outside of a cleanroom environment. The modified cutback method computes the average loss across many waveguides regardless of coupling variation, which makes the cutback measurement vulnerable to errors. While this issue can be mitigated with measuring a large number of samples, the intra-batch waveguide performance variation further motivates the use of the out-scattering method, which has the unique advantage of assessing the individual waveguide performance.

3.2 Out-Scattering Method Result

The out-scattering method results for one example waveguide were shown in Fig. 12, collected using the automated procedure described in Fig. 9. Sliding window sections with 1 mm intervals are taken along the waveguide path to produce localized measurements of the out-scattering method fitting propagation loss. This way, the localized propagation loss can be plotted along the distance from input port.

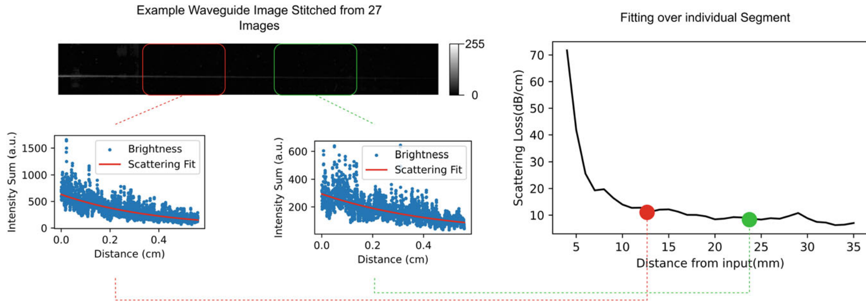

Fig. 12 Out-scattering method fitting processing for one waveguide. Multiple sections were imaged along the waveguide length for scattering fitting loss calculation. The results were aggregated to a single line in plot

For all Parylene photonic waveguides, a very high out-scattering fitting propagation loss around 80–100 dB/cm dominates the images captured near the input port, and declines very quickly until reaching 15 mm from the input port (Fig. 12). Prior work in the literature has also observed the same polymer waveguide propagation loss behavior [19]. The SNR of these images is in line with images further away from input port, which suggests that such a high loss is not introduced by stray light from the input port. We hypothesize that this is due to the higher-order modes which dominate near the input region of the waveguide as discussed in Sect. 2. Considering this loss is confined to the input region and does not scale with the waveguide length, we classify it as the insertion loss rather than propagation loss. Thus, the propagation losses obtained near the input region via the out-scattering method were not considered in the propagation loss evaluation.

In addition, the out-scattering method fitting is capable of identifying faulty waveguide regions by using the fitting R-Squared metric. Such faulty waveguide regions can result from a defect in the waveguide, fabrication imperfections or external debris on the surface of the waveguide, causing a localized outscattering of light. Faulty waveguide regions do not follow a standard out-scattering exponential decay, exhibiting a low R-Squared fitting. One example image having low R-Squared value is shown in Fig. 13a. In the corresponding out-scattering method fitting (Fig. 13b), two peaks are visible in the intensity profile which contribute to the low R-Squared value. Subsequent manual inspection of wafer surface revealed that the two intensity peaks are because of the surface debris on the waveguide which caused out-coupling of light from the waveguide. Thus, thresholding R-Squared value of out-scattering measurements can identify particles or debris affecting the waveguide. This method provides a promising direction for future quality control to detect variations in material quality and identify fabrication defects.

Furthermore, high SNR is also essential to ensure accurate out-scattering method fitting. Due to the exponential intensity decay, the brightness of out-scattering light decreases significantly along the waveguide propagation direction. Since the baseline noise level in the CCD camera is constant, the SNR decreases in proportion to the

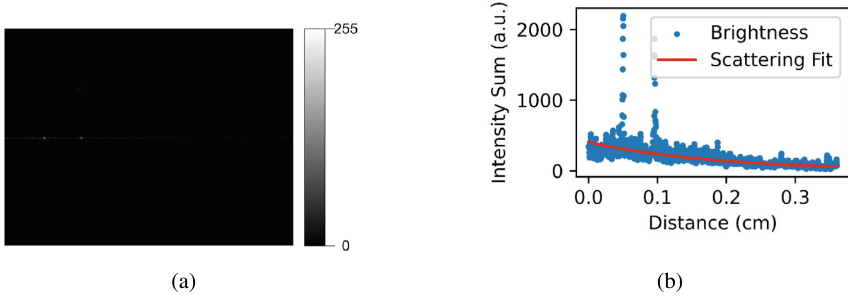

(a) (b)

Fig. 13 Example of R-squared threshold for defect detection. **a** Waveguide path image containing a faulty region. Two bright points on the waveguide path were identified to be surface debris causing out-coupling and optical power loss. **b** Out-scattering fitting of the left image. The fitting R-Squared value is 0.30, indicating a large deviation from an exponentially-decaying curve

decreasing out-scattering light intensity level. When SNR is low, the out-scattering method fitting curve will be affected by a uniform baseline noise, which tends to skew the fit and underestimate the actual propagation loss. In the following section, we provide an analytical relationship to illustrate the effect of low SNR. We assume a waveguide with true propagation loss α, an initial out-scattering intensity of I_0 at given length $L(z)$. Its out-scattering intensity at point z is given by

$$I(z) = I_0 e^{-\alpha L(z)}. \tag{6}$$

Then to model the impact of background noise, we assume noise as a positive half normal distribution with mean μ and variance σ^2 on intensity. The observed intensity is the sum of the two:

$$I(z) = I_0 e^{-\alpha L(z)} + |\mathcal{N}(\mu, \sigma^2)|. \tag{7}$$

Since the background noise is non-negative, we want to ensure a lower bound propagation loss $\eta\alpha$ where $0 < \eta < 1$ such that our observed intensity at that point will not be larger than a waveguide with propagation loss $\eta\alpha$. Its corresponding intensity is defined as the bounded intensity.

$$I_0 e^{-\alpha L(z)} + |\mathcal{N}(\mu, \sigma^2)| \leq I_0 e^{-\eta\alpha L(z))}. \tag{8}$$

Then at the given point L_0, the probability of the observed intensity being smaller than the bounded intensity is:

$$P(|\mathcal{N}(\mu, \sigma^2)| \leq I_0(e^{-\eta\alpha L(z)} - e^{-\alpha L(z)})). \tag{9}$$

This equation applies to every point L_0 over the imaged waveguide length L. The relationships between L, α, μ, and σ demonstrate the trends of fitting perfromance

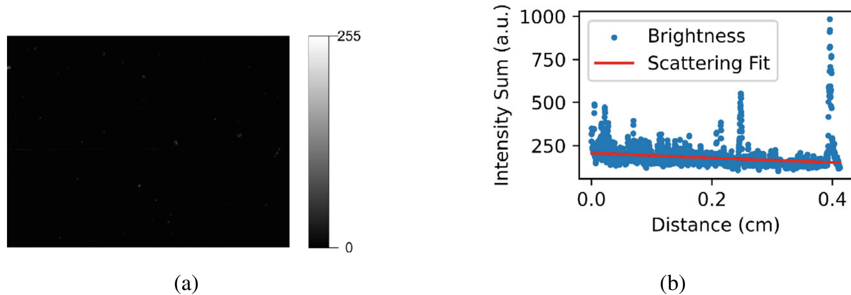

Fig. 14 Example of low-SNR image biasing out-scattering method fitting. **a** Waveguide path image containing low-SNR region. The background noisy spots have intensity comparable with waveguide path due to low SNR. **b** Out-scattering fitting of the left image. The fitting is dominated by background noise. The underestimated out-scattering fitting loss is 5.8 dB/cm

with background noise. Note that smaller propagation loss α and shorter imaging distance L are more easily skewed by background noise, requiring higher SNR.

As a numerical example to demonstrate the effect of background noise on loss fitting, we chose $L = 5.6\,\text{mm}$ and $\alpha = 10\,\text{dB/cm}$. For a distance x that is small, the value of exponential term $e^{-\alpha x}$ is close (1) Thus we can model an SNR of 20 by using a positive Gaussian noise model with zero mean and standard deviation $\frac{\sqrt{\pi}}{SNR \cdot \sqrt{2}}$ (which has an expected value of $\frac{1}{SNR}$):

$$I(x) = e^{-\alpha x} + |N(0, \left(\frac{\sqrt{\pi}}{SNR \cdot \sqrt{2}}\right)^2|$$

We simulated 10000 waveguides over L with 457 data points/mm to match our imaging system. We chose an η of 0.9 as the lower tolerance bound. In this setup, with a SNR of 20, 99.97% of the simulation trials produced an out-scattering propagation loss fitting result within the 10% error tolerance. Thus, with an SNR of 20, measurement results using the scattering method are highly unlikely (less than 0.01% chance) to deviate by more than 10% from the true value under the simulated conditions.

Consequently, to accurately perform out-scattering method measurements, the following steps should be followed:

(1) Imaging waveguides longer than 35 mm to maximize regions unaffected by near-input high loss, (2) excluding waveguides with R-Squared values lower than 0.4, and (3) excluding waveguide regions with SNR smaller than 20.

Figure 14 shows an example image with low SNR. The image is taken 35 mm from input port, where out-scattering light has decayed to a level difficult to detect even for the maximum camera exposure time. Here, the background noise skews the exponential decay, which results in a fitted propagation loss lower than estimation (5.8 db/cm versus 8.36 db/cm from the cutback method).

Seven 30 µm wide waveguides with lengths ranging from 35 mm to 50 mm passed the aforementioned criteria along their entire length. Their out-scattering

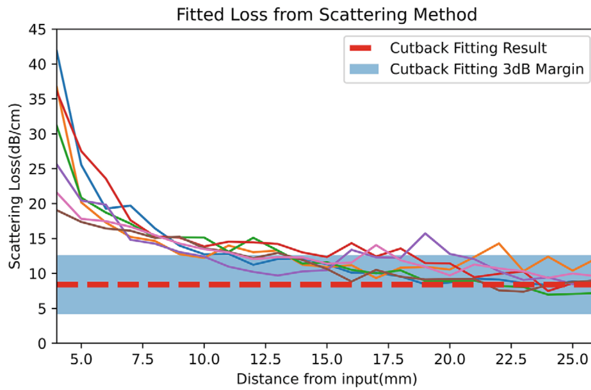

Fig. 15 Aggregated out-scattering method fitting result is shown above. 7 waveguides passing all aforementioned criteria are demonstrated in the plot. The majority of waveguide propagation losses converge within the 3 dB of modified cutback measurement after travelling 15 mm from input port

Table 1 Measurement time estimation for each waveguide

Step	Alignment 1–3	Imaging
Time (min)	2/ea	3–10

method fitting results are plotted for up to 27 mm from the input port (Fig. 15). The out-scattering method fitting for all qualifying waveguides have a majority of propagation losses stabilize to a value within the 3 dB of the cutback fitting result after travelling 15 mm from input port. This result demonstrates agreement between the the out-scattering fitting method compared to the gold-standard modified cutback method results.

The processing speed of the automated waveguide characterization system was also assessed. Since the light intensity captured by the camera during alignment is fixed, no exposure time adjustment is necessary in this phase. The time for each step is shown in Table 1, when the exposure time for each image is 0.5 s, the input coupling step takes 2 min each for three grid iterations and the automated waveguide imaging step takes 3 to 10 min for each waveguide depending on its length. On average, characterizing each waveguide takes around 15 min and the system can finish characterizing the propagation losses of 30 waveguides on a wafer in 12 hours. This is all done in an automated fashion using the custom-designed robotic system and after initializing the process, no human supervision is required.

4 Discussion

We have demonstrated an automated waveguide characterization system capable of measuring propagation loss of many (greater than fifty) waveguides without human intervention using either the out-scattering method or modified cutback method. The out-scattering fitting provides inherent advantages due to it's ability to characterize individual waveguides and provide a localized probe into individual waveguide propagation loss to detect faulty regions on the waveguide.

However, the out-scattering method is sensitive to multiple factors that have been identified and analyzed. Rapid out-scattering light decay due to the presence of higher-order modes overestimates the waveguide propagation loss near the input port. Particles and other defects skew the exponential fitting of intensity decay but can be automatically detected via a low R-squared value. Lastly, low SNR in the captured image can cause underestimation of measured propagation loss values, necessitating a suitably high SNR. Therefore, we define a set of quality metrics to ensure accurate measurements: (1) Imaging at least 15 mm from the input port, (2) R-squared value less than 0.4, (3) SNR greater than 20. A majority of waveguides propagation losses that satisfied our quality metrics converge within a 3 dB of the modified cutback measurement result. Therefore, under proper conditions, the out-scattering method provides a reliable assessment of propagation losses for waveguide samples compared to the gold-standard modified cutback method.

Two remaining limitations to the characterization system demonstrated here are the requirement for initial manual alignment of the fiber to the wafer and speed of imaging. Currently, the fiber must be manually lowered to the wafer surface and aligned to the first waveguide input port. Additional capabilities to perform coarse fiber alignment via computer vision detection of fiducal marks on the wafer surface, and proximity detection for the fiber to avoid collision would allow for wafers to be automatically loaded and unloaded in a production environment. Furthermore, the imaging speed may also be a bottleneck for the performance of the system in a high-throughput setting. The current 15-minute-per-waveguide trials may not scale well with foundry-level production speed. To increase the processing speed of automated alignment step, exposure time can be further reduced, at the cost of higher noise provided the waveguide path images are bright enough to maintain sufficient SNR. In addition, adopting a low-noise camera would reduce the need for a long integration time and expedite the acquisition process in automated characterization pipeline. Furthermore, there is a trade-off between the number of images taken on each waveguide and the acquisition time. Increasing the field of view for each image and reducing the overlap overlap between adjacent images during the automated imaging step is also a viable way to improve the throughput.